

Efficient High-Fidelity Flying Qubit Shaping

Benedikt Tissot^{*} and Guido Burkard[†]

Department of Physics, University of Konstanz, D-78457 Konstanz, Germany

Matter qubit to photonic qubit conversion is the cornerstone of numerous quantum technologies such as distributed quantum computing, as well as several quantum internet and networking protocols. We find the upper limit for the photonic pulse emission efficiency of arbitrary matter qubit states for imperfect emitters and show a path forward to optimize the fidelity. We formulate a theory for stimulated Raman emission which is applicable to a wide range of physical systems including quantum dots, solid state defects, and trapped ions, as well as various parameter regimes, including arbitrary pulse durations. Furthermore, the mathematical idea to use input-output theory for pulses to absorb the dominant emission process into the coherent dynamics, followed by a quantum trajectory approach has great potential to study other physical systems.

Efficient, tunable, and coherent quantum emitters are at the heart of many quantum technologies. Prominent examples include entanglement distribution [1, 2] as well as more general applications for quantum networks and communication [3–8] which can potentially enable a quantum internet [9, 10] with quantum-mechanically enhanced security and privacy. Additionally, single-photon emission represents a cornerstone for several photonic technologies [11–15]. Generally, there is a large interest in coherent quantum media conversion, as it allows the connection between different quantum systems with diverse properties. This enables hybrid quantum systems that combine the advantages of each subsystem. Such hybrid quantum systems can combine matter systems with beneficial properties for storage or computation, e.g. trapped ions [16], semiconductor qubits [17] implemented via quantum dots and defects in solids, or superconducting circuits [18], with easily transmittable photons [14]. In this regard, photons are the natural choice for traveling qubits [19] and can be used to exchange quantum states or create entanglement between distant matter systems.

Cavity-enhanced stimulated Raman emission is an established technique for controlled and (nearly) deterministic pulse emission, i.e. “push button-like” shaped pulse generation. This is of particular interest as it is a step towards making the emission and absorption more independent of each other which is of the utmost importance when exchanging states between diverse systems. The ability of Purcell enhancement to achieve a controllable emitter with high efficiency was already shown over a wide range of materials, e.g. trapped ions as well as atoms [20, 21], “un-trapped” atoms [22], quantum dots [23, 24], and defects in solids [25, 26]. Previous theoretical works found the solution of the adiabatic transfer [1, 27], as well as a pulse-shape independent limit for the transfer efficiency [28, 29] and the pulse-shape dependent limit for single-photon emission from a perfect emitter [30, 31].

In this paper we theoretically determine the fundamental limit of coherent state transfer for arbitrary pulse shapes from a stationary matter three-level-system (3LS)

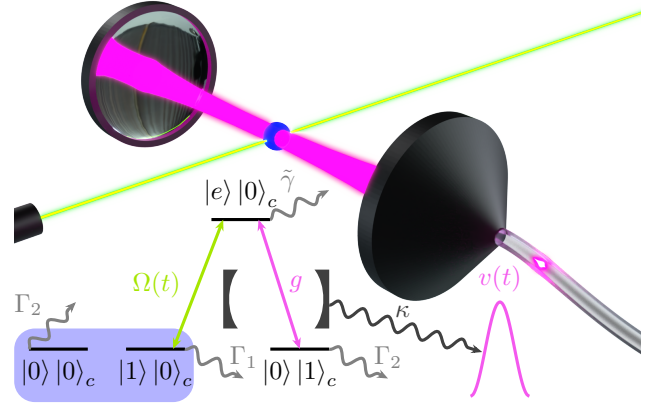


FIG. 1. Illustration of the physical system and energy level diagram of a stimulated Raman emitter. The illustration depicts a quantum system (blue ball) coupled to an electromagnetic cavity mode (pink) as well as an excitation (e.g. laser field) (green). One of the mirrors couples out into a fiber enabling the emission of a photon pulse (pink glowing droplet). The level diagram (bottom part) in the rotating frame depicts the excited state $|e\rangle$ (ES) split from the two ground states (GS) $|0\rangle$, $|1\rangle$ by the detuning Δ for the relevant states of the cavity $|0\rangle_c$ and $|1\rangle_c$ with zero and one photon. The matter qubit is given by the two ground states (blue shaded). The Lambda (Λ) system is set up by controllable time-dependent (excitation field) Rabi amplitude $\Omega(t)$ coupling $|1\rangle|0\rangle_c$ to the ES, as well as cavity interaction between the ES and $|0\rangle|1\rangle_c$ with single photon coupling strength g . The cavity emits the photon wave-packet with pulse shape $v(t)$ via the out-coupling κ . Imperfections of the three-level-system can lead to decoherence processes taken into account via the combined rates $\tilde{\gamma}$, Γ_1 , and Γ_2 .

via a cavity to a traveling qubit pulse. For simplicity we henceforth refer to the traveling qubit pulse as photon (wave-packet), the most prominent physical implementation. In particular, we are interested in the transfer of a superposition of *qubit states* $\alpha_0|1\rangle + \beta_0|0\rangle$ via the excited state $|e\rangle$ and cavity to the traveling photon $\alpha_0|1\rangle_v + \beta_0|0\rangle_v$, see Fig. 1.

The new found limit refines the previously known limits which only depend on the cavity decay rate and coop-

erativity of the emitter-cavity coupling, to include additional parameters of the cavity and the driven 3LS, most prominently different decoherence processes of the emitter as well as the *temporal shape of the flying qubit* $v(t)$ and initial superposition states, fundamentally necessary to understand spin-photon entanglement. Because the bound depends on the shape of the photon, it is suited to find optimized flying qubit shapes, providing an alternative to the shortcut to adiabaticity [32] approach as well as theories eliminating the propagating pulse completely [1]. We note that the stimulated Raman emission can also be used to create a photon entangled with the matter qubit, to transfer the matter qubit to a time-bin qubit, or to generate a time-bin qubit if an additional matter state is available to store the amplitude β_0 [see [33]].

We model the system in the rotating frame, where the Hamiltonian of the cavity interacting with the 3LS is $H_S/\hbar = \Delta |e\rangle \langle e| + [\Omega(t) |e\rangle \langle 1| + g c^\dagger |0\rangle \langle e| + \text{H.c.}]$, with the time-dependent Rabi frequency of the drive $\Omega(t)$, the detuning between the cavity and the $|0\rangle \leftrightarrow |e\rangle$ transition Δ , the 3LS states $|0\rangle, |1\rangle, |e\rangle$, and the cavity photon annihilation operator c . The energy level structure is sketched in Fig. 1. We absorbed the matter qubit splitting in $\Omega(t)$ in the rotating frame Hamiltonian. Additional details about the derivation of the rotating frame Hamiltonian can be found in the Supplemental Material [33].

To include the emission from the cavity into a specific output pulse in the Hermitian quantum dynamics we employ the recently developed input-output theory for quantum pulses [34, 35], where the dynamics are described using a *time-dependent master equation* of the form $\frac{d}{dt}\rho = -\frac{i}{\hbar}[H, \rho] + \sum_i \left(L_i \rho L_i^\dagger - \frac{1}{2} \{ L_i^\dagger L_i, \rho \} \right)$ with the (time-dependent) dissipators L_i that model various incoherent processes. The fundamental idea of this theory is to model the emission to the specific pulse as a *virtual cavity* with time-dependent coupling to the system such that the cavity would completely absorb the specific pulse. This is achieved by a total Hamiltonian $H = H_S + \hbar \frac{i}{2} \sqrt{\kappa} [g_v^*(t) c^\dagger a - \text{H.c.}]$, with the cavity decay rate κ , the annihilation operator of the virtual cavity a and time-dependent coupling strength $g_v(t) = -v^*(t)/\sqrt{\int_0^t dt' |v(t')|^2}$ which is directly linked to the normalized pulse form $v(t)$, i.e. $\int_0^T |v(\tau)|^2 d\tau = 1$ with the pulse duration T . Combined with the dissipator $L_0(t) = g_v(t)^* a + \sqrt{\kappa} c$, the total Hamiltonian leads to cascaded evolution, resulting in a transfer of the quantum amplitudes from the emitter to the virtual cavity. Additionally, a pulse shape that does not (perfectly) capture the dynamics of the emission process leads to incoherent losses via $L_0(t) \neq 0$ in the model.

To study the coherent state transfer of a matter state into the propagating wave packet, we focus on the single excitation subspace using a non-Hermitian Hamilto-

nian approach [36–39], described by the time-dependent Schrödinger equation $i\hbar \frac{\partial}{\partial t} |\Psi\rangle = H_{\text{NH}} |\Psi\rangle$ with $H_{\text{NH}} = H - \hbar \frac{i}{2} \sum_i L_i^\dagger L_i$ and using the ansatz wavefunction

$$|\Psi\rangle = \alpha |1\rangle |0\rangle_c |0\rangle_v + \beta |0\rangle |0\rangle_c |0\rangle_v + i\zeta |e\rangle |0\rangle_c |0\rangle_v + \eta |0\rangle |1\rangle_c |0\rangle_v + \lambda |0\rangle |0\rangle_c |1\rangle_v. \quad (1)$$

First we determine the optimal time-dependent coupling to the virtual cavity by solving $L_0 |\Psi\rangle = 0$ such that the emission is encoded in the Hermitian dynamics. This yields $g_v(t) = -\sqrt{\kappa} \eta^*(t)/\lambda^*(t)$ and corresponds to a perfect virtual impedance matching. Therefore the ideal case corresponds to a fully coherent process in our model. All remaining incoherent processes that bring the system out of the subspace spanned by the ansatz wavefunction describe unwanted losses. Therefore, we have immediate access to the probability of these errors $p_e = 1 - \langle \Psi(t) | \Psi(t) \rangle / \langle \Psi(0) | \Psi(0) \rangle \geq 0$ for $t \geq 0$, underlining that the chosen approach is perfectly suited to describe the coherent transfer of population. In the most relevant domain $p_e \ll 1$ the emission of multiple excitations is highly unlikely, further justifying the quantum trajectory approach.

Combining the impedance matching and the non-Hermitian Schrödinger equation the (decaying) dynamics of the coherent state transfer are

$$\dot{\alpha}(t) = -\frac{\Gamma_1}{2} \alpha(t) + \Omega^*(t) \zeta(t), \quad \dot{\beta}(t) = -\frac{\Gamma_2}{2} \beta(t), \quad (2)$$

$$\dot{\zeta}(t) = \left(-i\Delta - \frac{\tilde{\gamma}}{2} \right) \zeta(t) - g\eta(t) - \Omega(t) \alpha(t), \quad (3)$$

$$\dot{\eta}(t) = -\frac{\Gamma_2 + \kappa}{2} \eta(t) + g\zeta(t), \quad (4)$$

$$\dot{\lambda}(t) = -\frac{\Gamma_2}{2} \lambda(t) + \frac{\kappa |\eta(t)|^2}{2\lambda^*(t)}, \quad (5)$$

where we combined [33] important uncorrelated dephasing terms [40] and relevant decays from the states $|1\rangle$, $|0\rangle$, and $|e\rangle$ in the rates Γ_1 , Γ_2 , and $\tilde{\gamma}$, respectively.

To study these equations we first formally solve for the pulse amplitude $\lambda(t) = \sqrt{\kappa} e^{i\varphi} \sqrt{\int_0^t e^{\Gamma_2(\tau-t)} |\eta(\tau)|^2 d\tau}$ with the initial phase φ . Inserting this solution into the virtual impedance matching and comparing to the definition of $g_v(t)$ relates $\eta(t)$ to the pulse shape

$$\eta(t) = E |\alpha_0| e^{i\varphi} e^{-\Gamma_2 t/2} v(t) / \sqrt{\kappa}, \quad (6)$$

with $\alpha_0 = \alpha(0)$. We term the positive proportionality constant E the *matter-photon conversion efficiency* and demonstrate below that it is directly related to the fidelity of the process. Eq. (6) shows that the pulse shape is directly linked to the dynamics of the ES and combined with the virtual impedance matching we see that a static phase (such as φ) can be either encoded in $\lambda(t)$ and or $v(t)$. Reinserting into the photon probability amplitude

yields

$$\lambda(t) = E |\alpha_0| e^{i\varphi - \Gamma_2 t/2} \sqrt{\int_0^t |v(\tau)|^2 d\tau}. \quad (7)$$

Inspired by earlier results on the optimal control to emit a photon of a certain shape [30], we solve the remaining equations *in reverse* by imposing a fixed photon shape (and thereby η, λ). This approach leads us to

$$\zeta(t) = \frac{\Gamma_2 + \kappa}{2g} \eta(t) + \frac{1}{g} \dot{\eta}(t), \quad (8)$$

and the optimal drive

$$\Omega(t) = -\frac{(\tilde{\gamma}/2 + i\Delta)\zeta(t) + g\eta(t) + \dot{\zeta}(t)}{\alpha(t)}. \quad (9)$$

Because we can ensure that $|\alpha(t)| > 0$ for $0 \leq t < T$ if $\alpha_0 \neq 0$ and the form of $\Omega(t)$ is irrelevant for $\alpha_0 = 0$ as no emission takes place, this provides a solution of Eq. (3) for $\Omega(t)$. Additionally, we now choose φ such that $\Omega(t)$ becomes independent of the initial condition, i.e. $|\alpha_0| e^{i\varphi} = \alpha_0$ implying that the phase of α_0 becomes the phase of $\lambda(t)$. The complex phase of $\Omega(t)$ is then only influenced by the detuning Δ and the pulse shape $v(t)$.

The remaining Eq. (2) leads to the dynamics of $\alpha(t) = \alpha_0 r(t) e^{i\phi(t) - \Gamma_1 t/2}$, with $r(t), \phi(t) \in \mathbb{R}$ and $r(0) = 1$, $\phi(0) = 0$. We find the evolution $r\dot{r} = -\frac{1}{2}E^2\dot{G}$ where

$$\begin{aligned} \dot{G} = e^{t(\Gamma_1 - \Gamma_2)} \left\{ \left[1 + \frac{\tilde{\gamma} - \Gamma_2}{g^2} \left(\frac{\kappa}{4} + \frac{\dot{\theta}^2}{\kappa} \right) + \frac{2\ddot{\theta}\dot{\theta}}{\kappa g^2} \right] f^2 \right. \\ + \left(\frac{2}{\kappa} + \frac{\kappa}{2g^2} + \frac{\tilde{\gamma} - \Gamma_2}{g^2} + \frac{2\dot{\theta}^2}{\kappa g^2} \right) f\dot{f} \\ \left. + \left(\frac{1}{g^2} + \frac{\tilde{\gamma} - \Gamma_2}{\kappa g^2} \right) \dot{f}^2 + \frac{1}{g^2} f\ddot{f} + \frac{2}{\kappa g^2} \dot{f}\ddot{f} \right\}, \quad (10) \end{aligned}$$

with the photon envelope phase $\theta(t) \in \mathbb{R}$ and amplitude $f(t) \in \mathbb{R}$, i.e. $v(t) = e^{-i\theta(t)} f(t)$. In the equation we dropped the explicit time dependence of f, θ for brevity of the notation. As \dot{G} is independent of r , integrating both sides yields $r^2(t) = 1 - E^2 G(t) \geq 0$, with $G(t) = \int_0^t \dot{G}(\tau) d\tau$. Note that $r(t)$ and $G(t)$ are independent of the detuning Δ . Using $r(t)$ it is straight forward to calculate the phase dynamics $\phi(t)$ with another integration [33]. Here we note that $\phi(t)$ remains constant for a resonant cavity and a pulse shape with constant complex argument $\Delta = \dot{\theta}(t) = 0$. Another technical highlight is that $\Omega(t)$, $G(t)$, $r^2(t)$, and $\phi(t)$ are all independent of the initial state of the matter qubit.

The central results of this article are derived from the bound imposed on the efficiency E by the positivity of $r^2(t)$. This condition applies for all times t including the worst time such that we calculate the bound

$$E \leq E_{\max} = \frac{1}{\sqrt{\max_{t \geq 0} G(t)}}. \quad (11)$$

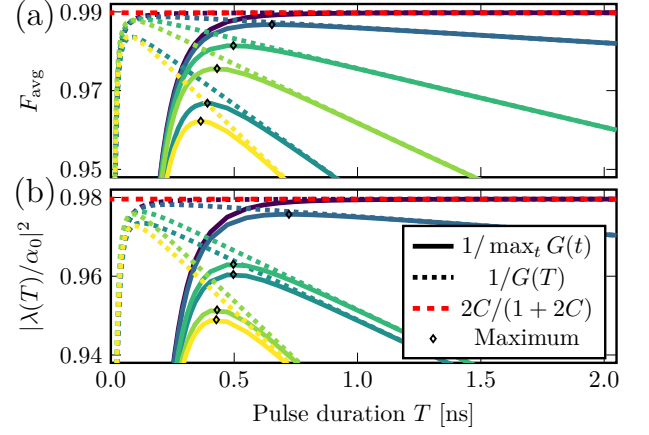


FIG. 2. Bounds for the average fidelity (a) and the amplitude transfer percentage (worst case fidelity) (b) as a function of the pulse duration for a \sin^2 pulse. We compare different limits, derived from different expressions for E^2 , the pulse form independent bound for the ideal emitter ($\Gamma_1, \Gamma_2 = 0$) $E^2 = 2C/(1 + 2C)$ (dashed red line), and the pulse form dependent fidelities based on the exact maximum $E^2 = 1/\max_t G(t)$ (solid lines), as well as the approximation $E^2 = 1/G(T)$ (dotted lines). The pulse form dependent bounds are shown for different decoherences of the matter qubit $(\Gamma_1, \Gamma_2)/\tilde{\gamma}$, from dark (blue) to light (yellow) the values are (0, 0), (0.01, 0.005), (0, 0.1), (0.1, 0), (0.2, 0), and (0.1, 0.1). For non-vanishing decoherence rates and short pulse durations we see significant deviations from the ideal bound that overestimates the bound in these cases. It is clearly visible that for imperfect emitters there is a maximal fidelity (diamonds) for a finite pulse duration. Additionally, it is visible that $G(T)$ gives a good approximation for $\max_t G(t)$ for long pulse durations. We use cavity QED parameters that can describe SiV defects in diamond (g, κ, γ) = $2\pi \times (6, 30, 0.1)$ GHz.

This implies that a varying phase in the rotating frame is detrimental, i.e., reduces E_{\max} , as long as $\Gamma_1 < \tilde{\gamma}$. To prove this we combine the partial integration $2 \int_0^t e^{(\Gamma_1 - \Gamma_2)t} [\dot{\theta}\ddot{f}^2 + \dot{\theta}^2 f\dot{f}]^2 dt = e^{(\Gamma_1 - \Gamma_2)t} f^2(t) \dot{\theta}^2(t) - (\Gamma_1 - \Gamma_2) \int_0^t \dot{\theta}^2 f^2 e^{(\Gamma_1 - \Gamma_2)t} dt$ with Eq. (10). This aligns with the intuition that a better phase control of the ES (limited by $\tilde{\gamma}$) is required to create a varying phase. The bound of the parameter E also limits the fidelity $F = |\alpha_0^* \lambda(T) + \beta_0^* \beta(T)|^2$ of the state transfer $[(\alpha_0 |1\rangle + \beta_0 |0\rangle) |0\rangle_c |0\rangle_v \rightarrow |0\rangle |0\rangle_c (\alpha_0 |1\rangle_v + \beta_0 |0\rangle_v)]$

$$F \leq e^{-\Gamma_2 T} |1 - (1 - E_{\max}) \alpha_0|^2, \quad (12)$$

or similarly the percentage of the amplitude transferred from $|1\rangle$ to $|1\rangle_v$

$$\left| \frac{\lambda(T)}{\alpha_0} \right|^2 = \frac{E^2}{e^{\Gamma_2 T}} \leq \frac{E_{\max}^2}{e^{\Gamma_2 T}}. \quad (13)$$

We note that $|\lambda(T)/\alpha_0|^2$ does not depend on the initial condition α_0 , and is equal to the worst-case fidelity

$F(|\alpha_0| = 1)$. This result is a generalization to the upper bound for the maximal efficiency in [30] where we stress that by incorporating the imperfections of the emitter the fidelity has a maximum for a finite time [see Fig. 2] and is therefore suited to optimize the pulse duration. Another fidelity independent of the initial state is the average fidelity. Averaging (12) over the Bloch sphere yields

$$F_{\text{avg}} = \frac{E^2 + E + 1}{3e^{\Gamma_2 T}} \leq \frac{E_{\text{max}}^2 + E_{\text{max}} + 1}{3e^{\Gamma_2 T}}. \quad (14)$$

Considering that by definition $\max_t G(t) \geq G(T)$ and $G(T) > 0$ if $\Gamma_1, \Gamma_2 < \kappa, \tilde{\gamma}$, i.e. the decoherence rates of the matter qubit are smaller than the cavity outcoupling and ES decoherence rate which is likely in implementations, we can use $G(T)$ as a “simpler” limit for Eqs. (12)–(14). In particular, for a slowly evolving pulse $\dot{\theta}, \dot{f} \ll \kappa, g$ and for $\Gamma_1 = \Gamma_2 = 0$ we find $E^2 \lesssim 2C/(1 + 2C)$, with the (generalized) cooperativity $C = 2g^2/\tilde{\gamma}\kappa$. This corresponds to the photon retrieval (and storage) efficiency found in previous works [28, 29] (without dephasing of $|e\rangle$). We emphasize that the photon envelope dependent bounds are more precise, not only taking the photon shape but also decoherence processes of the emitter into account.

To gain a better understanding of our results, we consider a pulse shape of the form

$$v(t) = f(t) = \sum_{n=1}^L f_n \left[1 - \cos\left(\frac{2\pi n}{T}t\right) \right] \quad (15)$$

which is real [$\theta(t) = 0$], symmetric, fulfills $f(0) = f(T) = \dot{f}(0) = \dot{f}(T) = 0$ [41], and contains L independent parameters $T, f_n/f_1$ with $n = 2, \dots, L$ as f_1 is fixed by normalization. For $L = 1$ this ansatz is a \sin^2 -pulse with variable pulse duration. While we focus on this form, other pulse forms, in particular non-symmetric ones, that are compatible with the initial conditions [only $\alpha(0), \beta(0) \neq 0$] can be investigated analogously.

We show the maximal percentage of the amplitude transfer $|\lambda(T)/\alpha_0|$ and average fidelity for $L = 1$ as a function of the pulse duration T in Fig. 2. This finding is of the utmost interest as it gives a useful bound for the maximal achievable fidelity for all possible timescales as well as detunings and does not rely on adiabatic approximations. The figure makes it readily visible that the new bounds capture the limited fidelity for short pulses due to the finite cavity coupling strength g , cavity decay rate κ , as well as the bound due to decoherence processes of the 3LS for long pulses. Combined, this leads to the existence of an optimal finite pulse duration. More generally, we can take an ansatz for the envelope and optimize its independent parameters with regard to any other relevant quantity limited by Eq. (11). For example maximizing the amplitude transfer percentage $|\lambda(T)/\alpha_0|$ [Eq. (13)]

corresponds to the optimization

$$(f, \theta)_{\text{opt}} = \underset{f, \theta}{\operatorname{argmax}} \frac{1}{\max_t e^{\Gamma_2 T} G(t)}, \quad (16)$$

where we aim to find the optimal pulse envelope $v(t) = f(t)e^{i\theta(t)}$ including the pulse duration T . By using an ansatz for $f(t), \theta(t)$ the optimization is over a parameter space instead of a function space, and the whole problem can be rewritten as a (continuous) minimax problem [42, 43] $\operatorname{argmin}_{\vec{f}, \vec{\theta}} \max_{0 < t < T} e^{\Gamma_2 T} G(t)$ which is a known optimization problem to find the optimal values for \vec{f} and $\vec{\theta}$.

Here, we use the ansatz in Eq. (15) [$\theta(t) = 0$] and employ a grid optimization to find the L optimal parameters $T, f_n/f_1$ ($n = 2, \dots, L$). We show optimized pulse shapes and the corresponding fidelity bounds in Fig. 3. It is also possible to fix any parameter and only optimize a subset; in particular, if the rate at which the drive can be modulated is larger than the optimal T we can fix it to the minimal achievable T and only optimize the shape of the photon.

Given the result of the optimization, we have immediate access to the photon shape as well as to the driving Rabi frequency to generate that pulse. From Eqs. (8) and (9) we see that $\dot{f}(0) \neq 0$ leads to $\Omega(0) \neq 0$. To avoid such an instant activation of the drive we can restrict our ansatz to $\dot{f}(0) = 0$ by only using odd n as free parameters and setting $f_{2n} = -\frac{n^2}{(n+1)^2} f_{2n-1}$. Furthermore, it is possible to smooth the driving Rabi frequency by reducing the target efficiency, i.e. $E/E_{\text{max}} < 1$. Both effects are shown in Fig. 3(d).

In conclusion, we derived a novel limit for the fidelity for cavity-assisted stimulated Raman emission, taking not only the cavity quantum electrodynamic quantities, but also the temporal pulse shape and additional decoherence processes of the 3LS into account. Furthermore, we showed how this new bound can be cast into an optimization problem for the pulse shape for an efficient emission process. We underline the importance of this optimization option for material independent quantum networks, in particular in combination with optimal photon absorption approaches [29]. The method of including the main emission process into the coherent dynamics by combining the novel input-output approach by [34, 35] with the quantum trajectory method should be applicable to many problems. A natural next step would be to study a photon mediated matter-to-matter transfer within this framework.

We acknowledge funding from the European Union’s Horizon 2020 research and innovation programme under Grant Agreement No. 862721 (QuanTELCO), as well as from the German Federal Ministry of Education and Research (BMBF) under the Grant Agreement No. 13N16212 (SPINNING).

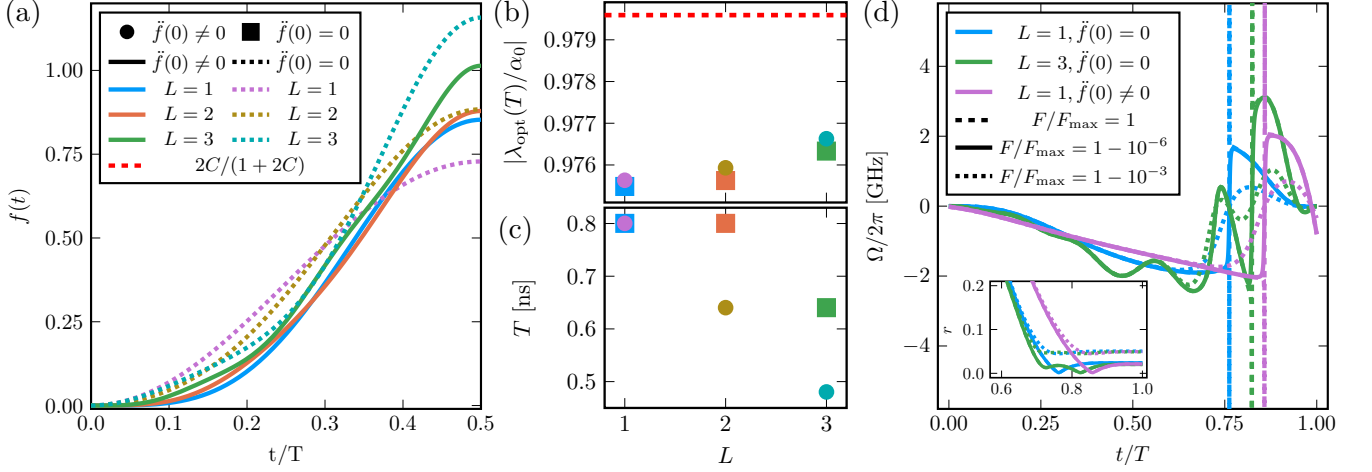


FIG. 3. Results of optimizing the pulse shape for maximal amplitude transfer. Panel (a) shows half of the optimal symmetric pulse shapes $f(t)$ for different numbers of free parameters L and restrictions on the pulse (see legend). The corresponding maximal transferred amplitude percentage $|\lambda_{\text{opt}}(T)/\alpha_0|^2$ and optimal pulse duration are depicted in panels (b) and (c). Parameters are those of Fig. 2 and $\Gamma_1 = \gamma/100$, $\Gamma_2 = \Gamma_1/2$. (d) Driving Rabi frequency $\Omega(t)$ as a function of time for different pulses and E/E_{max} (see legend). Reducing E leads to a larger minimal $|\alpha(t)| = e^{-\Gamma_2 t} r(t)$ (see inset) and smoothes out discontinuities in $\Omega(t)$. Parameters of Fig. 2, $\Delta = 0$ and for use 500 samples for T between $\min(1/\kappa, 1/g)/10$ and $\max(1/\Gamma_1, 1/\Gamma_2)/10$ (here ≈ 0.005 ns and 32 ns) and for each λ_n/λ_1 ($n = 2, \dots, L$) 200 samples between -1 and 1 .

* benedikt.tissot@uni-konstanz.de

† guido.burkard@uni-konstanz.de

- [1] J. I. Cirac, P. Zoller, H. J. Kimble, and H. Mabuchi, Quantum state transfer and entanglement distribution among distant nodes in a quantum network, *Physical Review Letters* **78**, 3221 (1997).
- [2] T. van Leent, M. Bock, F. Fertig, R. Garthoff, S. Eppelt, Y. Zhou, P. Malik, M. Seubert, T. Bauer, W. Rosenfeld, W. Zhang, C. Becher, and H. Weinfurter, Entangling single atoms over 33 km telecom fibre, *Nature* **607**, 69 (2022).
- [3] N. Gisin and R. Thew, Quantum communication, *Nature Photonics* **1**, 165 (2007).
- [4] K. Nemoto, M. Trupke, S. J. Devitt, A. M. Stephens, B. Scharfenberger, K. Buczak, T. Nöbauer, M. S. Everitt, J. Schmiedmayer, and W. J. Munro, Photonic architecture for scalable quantum information processing in diamond, *Phys. Rev. X* **4**, 031022 (2014).
- [5] W. J. Munro, K. Azuma, K. Tamaki, and K. Nemoto, Inside quantum repeaters, *IEEE Journal of Selected Topics in Quantum Electronics* **21**, 78 (2015).
- [6] F. Grasselli, H. Kampermann, and D. Bruß, Conference key agreement with single-photon interference, *N. J. Phys.* **21**, 123002 (2019).
- [7] W. Zhang, T. van Leent, K. Redeker, R. Garthoff, R. Schwonnek, F. Fertig, S. Eppelt, W. Rosenfeld, V. Scarani, C. C.-W. Lim, and H. Weinfurter, A device-independent quantum key distribution system for distant users, *Nature* **607**, 687 (2022).
- [8] D. P. Nadlinger, P. Drmota, B. C. Nichol, G. Araneda, D. Main, R. Srinivas, D. M. Lucas, C. J. Ballance, K. Ivanov, E. Y.-Z. Tan, P. Sekatski, R. L. Urbanke, R. Renner, N. Sangouard, and J.-D. Bancal, Experimental quantum key distribution certified by Bell's theorem, *Nature* **607**, 682 (2022).
- [9] H. J. Kimble, The quantum internet, *Nature* **453**, 1023 (2008).
- [10] S. Wehner, D. Elkouss, and R. Hanson, Quantum internet: a vision for the road ahead, *Science* **362**, nil (2018).
- [11] J. L. O'Brien, A. Furusawa, and J. Vučković, Photonic quantum technologies, *Nature Photonics* **3**, 687 (2009).
- [12] V. Giovannetti, S. Lloyd, and L. Maccone, Advances in quantum metrology, *Nature Photonics* **5**, 222 (2011).
- [13] A. Aspuru-Guzik and P. Walther, Photonic quantum simulators, *Nature Physics* **8**, 285 (2012).
- [14] S. Slussarenko and G. J. Pryde, Photonic quantum information processing: a concise review, *Applied Physics Reviews* **6**, 041303 (2019).
- [15] D. J. Brod, E. F. Galvão, A. Crespi, R. Osellame, N. Spagnolo, and F. Sciarrino, Photonic implementation of boson sampling: a review, *Advanced Photonics* **1**, 1 (2019).
- [16] C. D. Bruzewicz, J. Chiaverini, R. McConnell, and J. M. Sage, Trapped-ion quantum computing: Progress and challenges, *Applied Physics Reviews* **6**, 021314 (2019).
- [17] G. Burkard, T. D. Ladd, J. M. Nichol, A. Pan, and J. R. Petta, Semiconductor spin qubits, *CoRR* (2021), [arXiv:2112.08863 \[cond-mat.mes-hall\]](https://arxiv.org/abs/2112.08863).
- [18] M. Kjaergaard, M. E. Schwartz, J. Braumüller, P. Krantz, J. I.-J. Wang, S. Gustavsson, and W. D. Oliver, Superconducting qubits: Current state of play, *Annual Review of Condensed Matter Physics* **11**, 369 (2020).
- [19] C. H. Bennett and G. Brassard, Quantum cryptography: Public key distribution and coin tossing, *Theoretical Computer Science* **560**, 7 (2014), rEPRINT of a 1984 article.
- [20] A. Kuhn, M. Hennrich, and G. Rempe, Deterministic single-photon source for distributed quantum network-

- ing, *Phys. Rev. Lett.* **89**, 067901 (2002).
- [21] L.-M. Duan, A. Kuzmich, and H. J. Kimble, Cavity qed and quantum-information processing with "hot" trapped atoms, *Physical Review A* **67**, 032305 (2003).
- [22] P. B. R. Nisbet-Jones, J. Dille, D. Ljunggren, and A. Kuhn, Highly efficient source for indistinguishable single photons of controlled shape, *New J. Phys.* **13**, 103036 (2011).
- [23] T. M. Sweeney, S. G. Carter, A. S. Bracker, M. Kim, C. S. Kim, L. Yang, P. M. Vora, P. G. Brereton, E. R. Cleveland, and D. Gammon, Cavity-stimulated raman emission from a single quantum dot spin, *Nature Photonics* **8**, 442 (2014).
- [24] B. C. Pursley, S. G. Carter, M. K. Yakes, A. S. Bracker, and D. Gammon, Picosecond pulse shaping of single photons using quantum dots, *Nature Communications* **9**, 115 (2018).
- [25] S. Sun, J. L. Zhang, K. A. Fischer, M. J. Burek, C. Dory, K. G. Lagoudakis, Y.-K. Tzeng, M. Radulaski, Y. Kellaita, A. Safavi-Naeini, Z.-X. Shen, N. A. Melosh, S. Chu, M. Lončar, and J. Vučković, Cavity-enhanced raman emission from a single color center in a solid, *Phys. Rev. Lett.* **121**, 083601 (2018).
- [26] E. N. Knall, C. M. Knaut, R. Bekenstein, D. R. Assumpcao, P. L. Stroganov, W. Gong, Y. Q. Huan, P.-J. Stas, B. Machielse, M. Chalupnik, D. Levonian, A. Suleymanzade, R. Riedinger, H. Park, M. Lončar, M. K. Bhaskar, and M. D. Lukin, Efficient source of shaped single photons based on an integrated diamond nanophotonic system, *Phys. Rev. Lett.* **129**, 053603 (2022).
- [27] C. K. Law and H. J. Kimble, Deterministic generation of a bit-stream of single-photon pulses, *J. Modern Optics* **44**, 2067 (1997).
- [28] A. V. Gorshkov, A. André, M. D. Lukin, and A. S. Sørensen, Photon storage in Λ -type optically dense atomic media. I. cavity model, *Phys. Rev. A* **76**, 033804 (2007).
- [29] J. Dille, P. Nisbet-Jones, B. W. Shore, and A. Kuhn, Single-photon absorption in coupled atom-cavity systems, *Phys. Rev. A* **85**, 023834 (2012).
- [30] G. S. Vasilev, D. Ljunggren, and A. Kuhn, Single photons made-to-measure, *N. J. Phys.* **12**, 063024 (2010).
- [31] M. Khanbekyan and D.-G. Welsch, Cavity-assisted spontaneous emission of a single Λ -type emitter as a source of single-photon packets with controlled shape, *Phys. Rev. A* **95**, 013803 (2017).
- [32] A. Baksic, R. Belyansky, H. Ribeiro, and A. A. Clerk, Shortcuts to adiabaticity in the presence of a continuum: Applications to itinerant quantum state transfer, *Phys. Rev. A* **96**, 021801 (2017).
- [33] See attached supplemental material for the derivation of the rotating frame, a more detailed discussion of the decoherence rates, time-bin emission and entanglement generation via Raman emission and an ancillary state, the phase evolution of $\alpha(t)$, an example curve of $G(t)$, and the optimal pulse duration for a \sin^2 -pulse.
- [34] A. H. Kiilerich and K. Mølmer, Input-output theory with quantum pulses, *Phys. Rev. Lett.* **123**, 123604 (2019).
- [35] A. H. Kiilerich and K. Mølmer, Quantum interactions with pulses of radiation, *Phys. Rev. A* **102**, 023717 (2020).
- [36] J. Dalibard, Y. Castin, and K. Mølmer, Wave-function approach to dissipative processes in quantum optics, *Physical Review Letters* **68**, 580 (1992).
- [37] K. Mølmer, Y. Castin, and J. Dalibard, Monte carlo wave-function method in quantum optics, *J. Opt. Soc. Am. B* **10**, 524 (1993).
- [38] H. J. Carmichael, Quantum trajectory theory for cascaded open systems, *Phys. Rev. Lett.* **70**, 2273 (1993).
- [39] A. J. Daley, Quantum trajectories and open many-body quantum systems, *Adv. Phys.* **63**, 77 (2014).
- [40] J. Li, M. A. Sillanpää, G. S. Paraoanu, and P. J. Hakonen, Pure dephasing in a superconducting three-level system, *Journal of Physics: Conference Series* **400**, 042039 (2012).
- [41] J. M. Martinis and M. R. Geller, Fast adiabatic qubit gates using only σ_z control, *Phys. Rev. A* **90**, 022307 (2014).
- [42] B. Rustem and M. Howe, An approach to continuous minimax: the basic algorithm, *IFAC Proc. Volumes* **31**, 429 (1998).
- [43] B. Rustem and M. Howe, *Algorithms for Worst-Case Design and Applications to Risk Management* (Princeton University Press, 2009).

Supplementary Information: Efficient High-Fidelity Flying Qubit Shaping

Benedikt Tissot^{*} and Guido Burkard[†]

Department of Physics, University of Konstanz, D-78457 Konstanz, Germany

ROTATING FRAME AND LAB FRAME

Since the main text introduces the Hamiltonian in the rotating frame, in this section we link the rotating frame to the lab frame. The Hamiltonian in the lab frame is

$$\tilde{H}_S/\hbar = (\Delta + \omega_c) |e\rangle \langle e| - \delta |1\rangle \langle 1| + \omega_c c^\dagger c + \left(\tilde{\Omega}^*(t) |1\rangle \langle e| + g c^\dagger |0\rangle \langle e| + \text{H.c.} \right), \quad (\text{S1})$$

with the excited state energy $\Delta + \omega_c$ (in units of frequency), the qubit level splitting δ , the cavity frequency ω_c . We then apply the transformation to the rotating frame

$$U = \exp \left[-i(-\delta |1\rangle \langle 1| + \omega_c |e\rangle \langle e| + \omega_c c^\dagger c) t \right], \quad (\text{S2})$$

leading to

$$H_s/\hbar = U^\dagger \tilde{H}_S/\hbar U - iU^\dagger \dot{U} = \Delta |e\rangle \langle e| + (\Omega^*(t) |1\rangle \langle e| + g c^\dagger |0\rangle \langle e| + \text{H.c.}), \quad (\text{S3})$$

corresponding to the Hamiltonian of the main text. The detuning is Δ and the drive in the lab frame is linked to the rotating frame by $\tilde{\Omega}(t) = \Omega(t) \exp[-i(\delta + \omega_c)t]$. Additionally, we see how the splitting between the qubit states is absorbed in the time-dependent drive.

Using the same transformation we can also link the time-dependence of the coupling to the virtual cavity $\tilde{g}_v(t) = g_v(t) e^{i\omega_c t}$ between the lab and rotating frames. This also links the photon envelopes $\tilde{v}(t) = e^{-i\omega_c t} v(t)$ and leads to the correct transformation of the dissipator L_0 . Because the remaining dissipators only gain a global phase in the rotating frame and always occur in pairs (with their adjoint) in the master equation, we can treat the remaining dissipators as unchanged in the rotating frame.

DECOHERENCE RATES

In this section we show how to derive the combined decoherence rates arising in the non-Hermitian Hamiltonian from established dissipators from the Lindblad master equation. As mentioned in the main text we start with the time-dependent Lindblad master equation of the form

$$\frac{d\rho}{dt} = -\frac{i}{\hbar} [H, \rho] + \sum_i \left(L_i \rho L_i^\dagger - \frac{1}{2} \{ L_i^\dagger L_i, \rho \} \right), \quad (\text{S4})$$

In addition to the main dissipator L_0 introduced in the main text we consider the following dissipators:

- Decays from the excited state (ES) $|e\rangle$ to the ground states (GS) $|1\rangle, |0\rangle$: $L_1 = \sqrt{\gamma} \cos(\xi) |1\rangle \langle e|$, $L_2 = \sqrt{\gamma} \sin(\xi) |0\rangle \langle e|$ with the branching angle ξ
- The important uncorrelated dephasing terms [S1], here the dephasing of $|1\rangle$ and $|e\rangle$ using the phase of $|0\rangle$ as reference: $L_3 = \sqrt{\Gamma_{\text{ph}}^1} |1\rangle \langle 1|$ and $L_4 = \sqrt{\Gamma_{\text{ph}}^e} |e\rangle \langle e|$
- Incoherent transitions between the GSs: $L_5 = \sqrt{\Gamma_{0 \rightarrow 1}} |1\rangle \langle 0|$, $L_6 = \sqrt{\Gamma_{1 \rightarrow 0}} |0\rangle \langle 1|$

The effect of these dissipators on the non-Hermitian Schrödinger equation

$$i\hbar \frac{\partial}{\partial t} |\Psi\rangle = H_{\text{NH}} |\Psi\rangle = \left(H - \hbar \frac{i}{2} \sum_i L_i^\dagger L_i \right) |\Psi\rangle \quad (\text{S5})$$

only depends on $L_i^\dagger L_i$. This implies we can combine $\sum_{i=1,2,4} L_i^\dagger L_i = \tilde{\gamma} |e\rangle \langle e|$ with $\tilde{\gamma} = \gamma + \Gamma_{\text{ph}}^e$ and $\sum_{i=3,6} L_i^\dagger L_i = \Gamma_1 |1\rangle \langle 1|$ with $\Gamma_1 = \Gamma_{1 \rightarrow 0} + \Gamma_{\text{ph}}^1$. In the main text we refer to $\Gamma_{0 \rightarrow 1} = \Gamma_2$ for a consistent and simpler notation.

TIME-BIN EMISSION AND ENTANGLEMENT GENERATION

With an additional ancillary level or qubit we can use (cavity-enhanced) stimulated Raman emission to create qubit-photon entanglement or time-bin emission. The fundamental idea is to store the wavefunction amplitude β_0 (of qubit state $|0\rangle$) in an ancillary state during the emission from the qubit state $|1\rangle$ to the first time-bin $|1\rangle_1$. This is compatible with the solution in the main text, as the solution holds as long as $\zeta(0) = \eta(0) = \lambda(0) = 0$. After the first emission gates between the qubit and the ancillary state(s) are applied such that after another emission process the qubit state is encoded in two time-bins, i.e. a time-bin qubit with the state $\alpha_0 |1\rangle_1 + \beta_0 |1\rangle_2$. The indices label the time-bins which are independent pulses, i.e. pulses that have non-overlapping envelopes.

In Fig. S1 we show two examples implementing this idea, one for an ancillary qubit and one for a single ancillary state. For the ancillary qubit we need the two-qubit CNOT and SWAP gates while for the single additional state $|a\rangle$ we need the ability to apply a $\pi/2$ rotation between $|0\rangle$ and $|a\rangle$ in both cases an X gate between $|0\rangle, |1\rangle$ is necessary as well. The EMIT gate corresponds to the stimulated Raman emission process. In

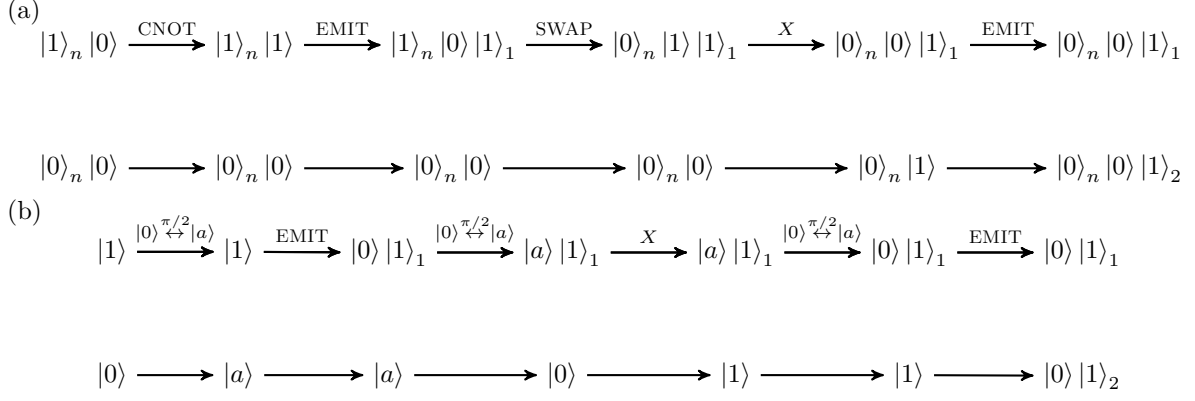


FIG. S1. Emission of a time-bin qubit using (a) an ancillary (e.g. nuclear spin) qubit or (b) an ancillary state. The main focus of the main text is the particular implementation of the EMIT process via cavity-enhanced stimulated Raman emission. CNOT and SWAP refer to the two qubit gates between the matter qubit and the ancillary qubit and X denotes the one-qubit X -gate of the matter qubit (or a $\pi/2$ -pulse between $|0\rangle$ and $|1\rangle$). Additionally, if one only implements the protocol up to the first emission, matter-photon entanglement is achieved.

both cases, stopping the protocol after the first emission can be used to generate entanglement. The created entangled states are $\alpha_0 |1\rangle_n |1\rangle_1 + \beta_0 |0\rangle_n |0\rangle_1$, where $|\sigma\rangle_n$ with $\sigma = 0, 1$ is the state of the ancillary qubit and $|m\rangle_1$ with $m = 0, 1, \dots$ is the number state of the first emitted pulse or $\alpha_0 |0\rangle_n |1\rangle_1 + \beta_0 |a\rangle_n |0\rangle_1$ using only one ancillary state $|a\rangle$.

Analogously, initializing the system in one of the ancillary states and then repeating a (partial) transfer of occupation to $|1\rangle$ followed by an emission enables time-bin qubit generation.

PHASE EVOLUTION OF $\alpha(t)$

In the main text we used a separation ansatz for $\alpha(t) = \alpha_0 r(t) e^{i\phi(t) - \Gamma_1 t/2}$ to determine the evolution of the rescaled absolute value $r(t)$ via a straight forward integral [see Eq. (10)]. After solving this integral the phase evolution also becomes a straight forward integral, i.e.

$$\begin{aligned} \dot{\phi} = \frac{E^2}{g^2 r^2} \left\{ \left[\frac{\kappa(\Delta + \dot{\theta})}{4} + \frac{\ddot{\theta}}{2} + \frac{\Delta\ddot{\theta}^2 - g^2\dot{\theta} + \dot{\theta}^3}{\kappa} \right] f^2 \right. \\ \left. + \left(\Delta + \dot{\theta} + \frac{\ddot{\theta}}{\kappa} \right) f\dot{f} + \frac{\Delta + 2\dot{\theta}}{\kappa} \dot{f}^2 \right. \\ \left. - \frac{\dot{\theta}}{\kappa} f\ddot{f} \right\} e^{(\Gamma_1 - \Gamma_2)t}. \end{aligned} \quad (\text{S6})$$

We can read off from this expression that $\dot{\phi}$ vanishes for $\Delta = 0$ and $\dot{\theta}(t) = 0$, implying that the phase ϕ is constant for $\Delta = 0$ and $\dot{\theta}(t) = 0$, i.e. a resonant cavity and a pulse shape with constant complex argument.

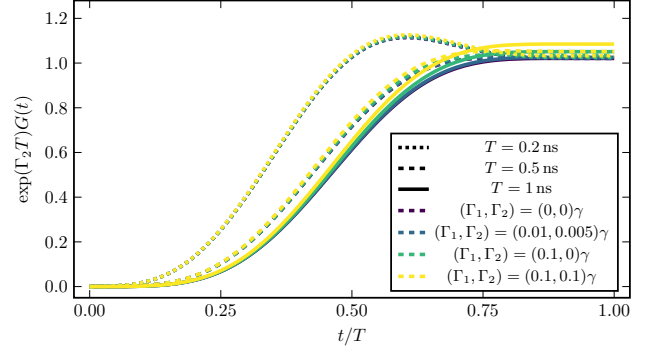


FIG. S2. Plots of $G(t)$ from Eq. (S7) used to calculate the maximally achievable fidelity for a set of parameters. We use the parameters of Fig. 2 of the main text.

TIME-DEPENDENCE OF $G(t)$ FOR A SIN^2 -PULSE

In this section we show the time dependence of $G(t)$ [see Eq. (10) of the main text] for a sin^2 pulse and for different decoherence rates. For convenience we repeat the dependence of $G(t)$ on the physical quantities here,

$$G(t) = [1 - r^2(t)]/E^2, \quad (\text{S7})$$

where $r^2(t) = e^{\Gamma_1 t} |\alpha(t)|^2 / |\alpha_0|^2$ and $\alpha(t)$ being the probability amplitude pertaining to the state $|1\rangle$ that is emitted into the photon pulse. As shown in the main text, at the same time we can derive a simple integrable expression for \dot{G} that depends on the shape of the photon pulse. Therefore, given a pulse shape, e.g. a sin^2 -pulse of fixed duration T , we can directly calculate $G(t)$. We also remind the reader that in combination with the positivity of $r^2(t)$, the function $G(t)$ limits the maximally

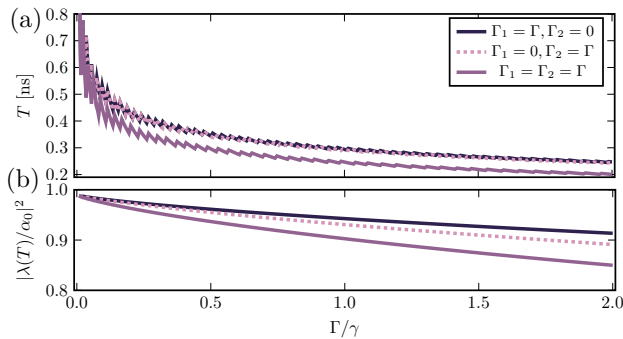


FIG. S3. Optimal pulse duration T for $L = 1$ and maximal probability transfer $|\lambda(T)/\alpha_0|^2$ as functions of the matter qubit decoherence. The colors correspond to different decoherence processes, see legend. We use the parameters of Fig. 2 of the main text.

achievable E and therefore the fidelity and probability transfer of the emission.

In Fig. S2 we show $\exp(\Gamma_2 T)G(T)$ for \sin^2 pulses of different duration and for different decoherence rates of the emitter. The figure visualizes how for long pulse durations the difference between $G(T)$ and $\max_t G(t)$ becomes smaller. It is also readily visible that for short pulses the maximum deviates from $G(T)$.

OPTIMAL PULSE DURATION

In the main text we showed examples of optimized pulses as well as the optimal pulse durations in Fig. 2.

Here, we want to expand on this result where for the simple case of a \sin^2 -pulse (using the basis of the main text $\lambda_i = 0$ for $i > 1$) the only variable parameter is the pulse duration T . We can therefore simply find the optimal pulse duration for a set of parameters.

We show the decay of the worst case fidelity as well as the decrease of the optimal duration as a function of the decoherence rates of the matter system in Fig. S3. The duration decrease flattens for higher rates as the duration is also limited from below due to the finite coupling between the matter-qubit and the cavity and out-coupling rate of the cavity. Furthermore we see that qualitatively the rates Γ_1, Γ_2 behave similar. But depending on the protocol of interest it might be preferential to swap the roles of $|0\rangle$ and $|1\rangle$, i.e. couple the shorter or longer lived state to the excited state via the cavity.

* benedikt.tissot@uni-konstanz.de

† guido.burkard@uni-konstanz.de

[S1] J. Li, M. A. Sillanpää, G. S. Paraoanu, and P. J. Hakonen, Pure dephasing in a superconducting three-level system, *Journal of Physics: Conference Series* **400**, 042039 (2012).